The fabrication of a chemical sensor with PANI-TiO$_2$ nanocomposites

Mohammad R. Karim,[ab] M. M. Alam, [ID] *[c] M. O. Aijaz,[a] Abdullah M. Asiri, [ID] [d] F. S. AlMubaddel[e] and Mohammed M. Rahman [ID] [d]

In this study, conjugated conducting polyaniline was fabricated onto titania nanoparticles (PANI-TiO$_2$ NPs) using a microwave-accelerated reaction system. The synthesized nanoparticles were characterized using the techniques of electron microscopy (*e.g.*, FE-SEM and TEM), X-ray diffraction (XRD), Fourier-transform infrared spectroscopy (FT-IR), and ultraviolet-visible (UV-Vis) spectrometry. An ultrasensitive sensor using the electrochemical ($I-V$) approach was fabricated using a thin film of PANI-TiO$_2$ NPs on a glassy carbon electrode (GCE), and it was found to be selective towards 1,2-diaminobenzene (1,2-DAB) in a buffer phase. From current *versus* concentration studies, the calibration curve was plotted to estimate the sensor's analytical parameters. The highest sensitivity (19.8165 μA μM^{-1} cm^{-2}) and lowest detection limit (0.93 ± 0.05 pM) were obtained from the electrochemical assessment by applying a signal-to-noise ratio of 3. A linear calibration plot was attained over a large range of concentration (LDR: 1.0 pM to 0.01 mM). The selective 1,2-DAB sensor was found to be efficient and reproducible in performance, yielding significant results with a fast response time (12.0 s). Therefore, the overall results of the 1,2-DAB chemical sensor suggest that this detection approach might be an easy way to develop an efficient electrochemical sensor for the protection of the environment as well as for use in the healthcare field on a broad scale.

Introduction

Generally, conductive polymers (CPs) are interesting materials for their distinctive properties and possible uses in numerous applications such as sensing, electronics, energy harvesting, and many more.[1–3] Among the CPs, polyaniline is widely used for its brilliant properties, such as excellent conductance, easy preparation, low cost, ecological friendliness and stability, and its redox characteristics in the N$_2$ backbone.[4,5] The reversibly tunable redox properties allow control of PANI's conductance over a broad range by protonation and doping charge-transfer systems. PANI is a classic phenylene polymer with a bendable amino group in the backbone.[6,7] Titania (TiO$_2$) is widely used due to its excellent properties for application in different fields, such as coatings, solar cells, and photocatalysts.[8] Therefore, a PANI-TiO$_2$ NP electrode may have good electrochemical

tendency and relatively high amount of reactive surfaces to improve the activity of target sensors.

The organic amine 1,2-DAB is a widely used industrial chemical intermediate. A number of industrial applications for 1,2-DAB produces a wide range of end products, such as dyes, pigments, medicines, auxiliaries, pesticides, photosensitive materials, and an intermediate of fungicides.[9] Exposure to 1,2-DAB through ingestion, inhalation and contact with the eyes may cause hazardous health effects on humans. Higher levels of 1,2-DAB concentration in humans is responsible for damaging the liver and respiratory and digestive systems, and it can also lead to cancer in humans. Therefore, numerous research studies have claimed that 1,2-DAB has mutagenic and carcinogenic effects in humans.[10,11] Besides this, 1,2-DAB is suspected as a serious environmental pollutant. On consideration of the health and environmental effects of 1,2-DAB, the American Conference of Governmental Industrial Hygienists (ACGIH) has declared 1,2-DAB carcinogenic and environmentally hazardous.[12] Based on these circumstances, the development of a consistent and convenient technique is urgently necessary for the efficient detection of 1,2-DAB in the environment as well as in the health sector. Presently, the existing analytical methods, such as high-performance liquid chromatography (HPLC),[13,14] spectrophotometry[15] and capillary electrophoresis (CE),[16] are used to detect 1,2-DAB. Considering the cost, time of analysis, heavy instrumentation and portability, these methods are not convenient for detecting 1,2-DAB.[17] Nowadays, research in the electrochemical

[a]Center of Excellence for Research in Engineering Materials (CEREM), King Saud University, Riyadh 11421, Saudi Arabia

[b]K.A.CARE Energy Research and Innovation Center, Riyadh 11451, Saudi Arabia

[c]Department of Chemical Engineering and Polymer Science, Shahjalal University of Science and Technology, Sylhet 3100, Bangladesh. E-mail: alam-mahmud@hotmail.com

[d]Center of Excellence for Advanced Materials Research & Chemistry Department, Faculty of Science, King Abdulaziz University, Jeddah 21589, Saudi Arabia

[e]Chemical Engineering Department, King Saud University, Riyadh 11421, Saudi Arabia

(I–V) method has confirmed the detection of a number of toxic chemicals while overcoming the disadvantages of other existing analytical methods.[18–23] Therefore, the objective of this research is to develop an electrochemical sensor using PANI-TiO$_2$ NPs on GCE.

Herein, an electrochemical sensor was developed using PANI-TiO$_2$ NPs coated onto GCE with a conducting Nafion membrane and applied to detailed investigation of its properties, such as selectivity, concentration variation, reproducibility, response time, and the examination of real environmental samples. Calibration using current versus concentration of 1,2-DAB was plotted to calculate the sensitivity, LOD, response time, linearity, and LDR of the proposed electrochemical sensor.

Experimental section

Resources and methods

Monomer (aniline, 99%), titania (∼20 nm), ammonium persulfate, hydrochloric acid and other solvents were purchased from Sigma-Aldrich as reagent grade. To complete the detailed investigation of this research, toxic chemicals such as 1,2-diaminobenzene (1,2-DAB), 2,4-diaminophenol (2,4-DAP), 2,4-diaminophenyl dihydrochloride (2,4-DAPDHCl), 2,4-dinitrophenol (2,4-DNP), 2-aminophenol (2-AP), 3,4-diaminotoluene (3,4-DAT), 3-methoxyphenol (3-MP), 4-aminophenol (4-AP), phenylhydrazine (PHyd), and p-nitrophenol (p-NP) were acquired and used without further purification.

Preparation of PANI-TiO$_2$ NPs

The PANI-TiO$_2$ NPs were synthesized with a routine synthesis method using microwave-accelerated reaction technique. Firstly, 1.5 mL of aniline monomer with the required amount of TiO$_2$ nanopowder was mixed in 25.0 mL of 1.0 M hydrochloric acid solution under 30 min sonication. Secondly, 0.1 M ammonium persulphate (APS) in 25.0 mL of 1.0 M hydrochloric acid solution was dropped slowly to the resultant blend, and the solution was transferred into a Teflon vessel for reacting in the microwave system (Mars-5, CEM, USA) at 75 °C for 15 min. Thirdly, it was cooled to room temperature. Finally, the PANI-TiO$_2$ NP powder was filtered by washing with DI water, acetone, ethanol, and 1.0 M hydrochloric acid. It was dried under vacuum at 45 °C overnight for further characterizations and use as chemical sensor material.

Fabrication of GCE with PANI-TiO$_2$ NPs

To develop the electrochemical sensor, a slurry of PANI-TiO$_2$ NPs was prepared in ethanol and used to coat onto GCE as a thin-film layer of NPs, then kept at ambient laboratory conditions to dry. For the desired binding strength of the PANI-TiO$_2$ NP film on CGE, a few drops of 5% Nafion suspension in ethanol were added onto the NP layer of the modified GCE. Then, it was kept in an oven at 35 °C for an hour to entirely dry the modified GCE. The proposed electrochemical sensor used was a Keithley electrometer (USA), where the assembled PANI-TiO$_2$ NPs/binder/GCE was used as working electrode and a Pt-wire was used as counter electrode. The 1,2-DAB solutions in deionized water, ranging 0.1 mM to 1.0 pM, were prepared and implemented as analyte. The current versus concentration data were used to plot a calibration curve, and the slope of the calibration plot was significantly utilized to measure the analytical parameters (sensitivity, LDR, linearity, and detection limit) of the proposed electrochemical sensor. Considering the maximum regression coefficient (R^2) value in the calibration plot, the linear dynamic region (LDR) was selected. Throughout the detailed electrochemical (I–V) investigation, the phosphate buffer solution in the measurement beaker was kept constant at 10.0 mL.

Instrumentation

To evaluate the morphology of PANI and PANI-TiO$_2$ NPs, a transmission electron microscope (TEM: JSM-2100F, JEOL, Japan) and field-emission scanning electron microscope (FESEM: JSM-7600, JEOL, Japan) were used. The functional groups of the prepared NPs were identified using the Fourier-transform infrared (FTIR: Vertex-70, Bruker, USA) and UV-Vis-NIR spectrometer (Shimadzu UV-Vis-NIR 3600, Japan). The powder X-ray diffraction (XRD: Bruker D8 Discover) was used to determine phase crystallinity and the average particle size. The detailed electrochemical (I–V) studies were executed using a Keithley electrometer (USA) with PANI-TiO$_2$ NPs/Nafion/GCE and Pt-wire as working and counter electrodes, respectively.
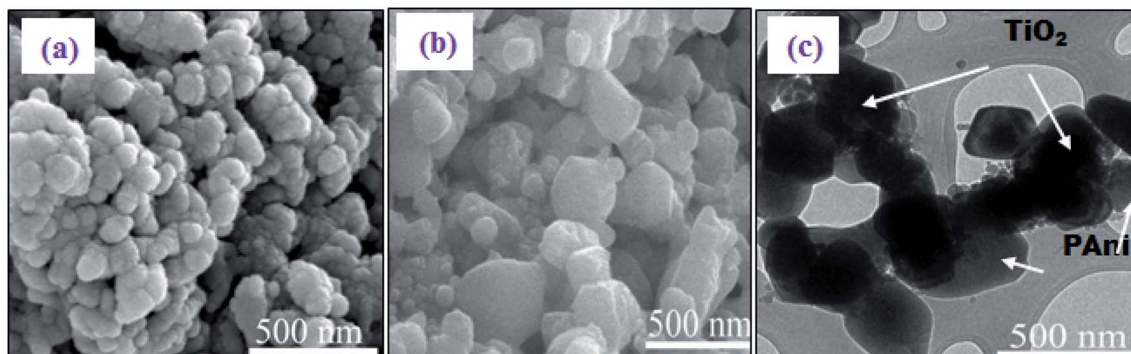

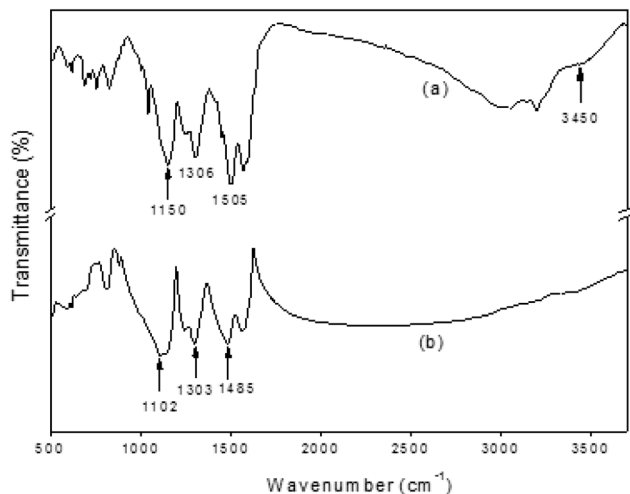Fig. 1   FESEM images of (a) PANI and (b) PANI-TiO$_2$ NPs. (c) A TEM image of PANI-TiO$_2$ NPs.

Fig. 2 FTIR results for (a) PANI and (b) PANI-TiO$_2$ NPs.

Results and discussion

FESEM and TEM analysis of PANI-TiO$_2$ NPs

The PANI-TiO$_2$ NPs were identified using the FESEM and TEM techniques, as shown in Fig. 1. The morphology of pure PANI is displayed in Fig. 1(a). From Fig. 1(b), the PANI-TiO$_2$ NPs show a different morphology from pure PANI due to the presence of TiO$_2$ in the composites. The calculated diameter of the PANI-TiO$_2$ NPs, which were successfully fabricated by the microwave-accelerated reaction system, ranges from 70 nm to 250 nm. The TEM image in Fig. 1(c) also supports the FESEM morphology that the inorganic nanoparticles (*i.e.* TiO$_2$) are attached to the organic counterparts (*i.e.*, PANI), as indicated in the picture.

FTIR and UV-Vis spectroscopy analysis

Fig. 2 presents the FTIR data for the bulk PANI powder and the PANI-TiO$_2$ NPs. In the case of PANI powder, in Fig. 2(a), the data agree with the published values.[15,24,25] The peaks at 1505 and 1576 cm^{-1} reveal the characteristic elongation of C=C for the

benzenoid and quinoid rings, respectively. At the 980–1175 cm^{-1} region, generally aromatic C–H in-plane peaks are found. Further, at 1306 cm^{-1}, the C–N stretching peak of the secondary aromatic amine, and at 828 cm^{-1}, the aromatic C–H out-of-plane bending vibration peaks, could be assigned. The results give clear evidence that PANI was developed in the products. From Fig. 2(b), all PANI peaks appear as well for the PANI-TiO$_2$ NPs in the 700–1600 cm^{-1} region, but the relative intensities of some peaks have changed/shifted due to the inclusion of TiO$_2$ NPs. Some examples of shifted peaks include those from 1505 to 1485 and 1306 to 1303 cm^{-1}, and the doping-related PANI peak is also shifted from 1150 to 1102 cm^{-1}. This indicates that interactive relations might have occurred between the PANI-TiO$_2$ NPs. Also, titania is a transition metal, and it has a strong affinity for coordination bonding with the N$_2$ molecule of polyaniline.[24]

UV-Vis spectroscopy was used to evaluate the optical behaviors of pure PANI and PANI-TiO$_2$ NPs in *N*-methyl-pyrrolidinone solutions. From Fig. 3(a), the pure PANI powder gives peaks at 320 and 596 nm due to the π–π* transition of benzene rings and quinoid exciton, respectively.[26] There are blue-shifting peaks found from 595 nm to 580 nm and from 322 nm to 295 nm, which indicate the existence of titania with the PANI oxidation states in the polymerization process of PANI-TiO$_2$ NPs. The relative intensities were also changed, confirming that the interaction between PANI and TiO$_2$ was kept, which decreases the degree of orbital overlap between the π-electrons of phenyl rings with the lone pair of N$_2$ atoms. At the same time, the peaks were shifted because PANI conjugation decreased.[27]

Powder X-ray diffraction pattern of PANI-TiO$_2$ NPs

The XRD data for PANI, TiO$_2$ and PANI-TiO$_2$ NPs are given in Fig. 4. Pure PANI shows a broad peak in the region of $2\theta = 20$–$50°$, with some degree of crystallinity corresponding to (100) and (110) planes [JCPDS no. 53-1718].[1] Bulk TiO$_2$ clearly shows corresponding peaks to the planes (101) (211) (220) (112) at $2\theta = 30$–$80°$. Comparison of pure PANI, bulk TiO$_2$ and the PANI-TiO$_2$
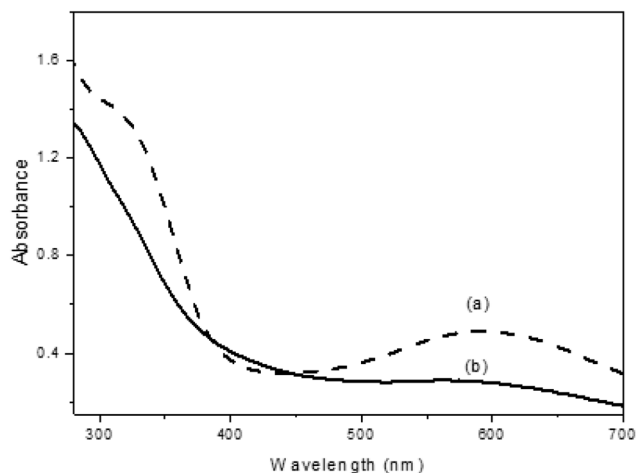

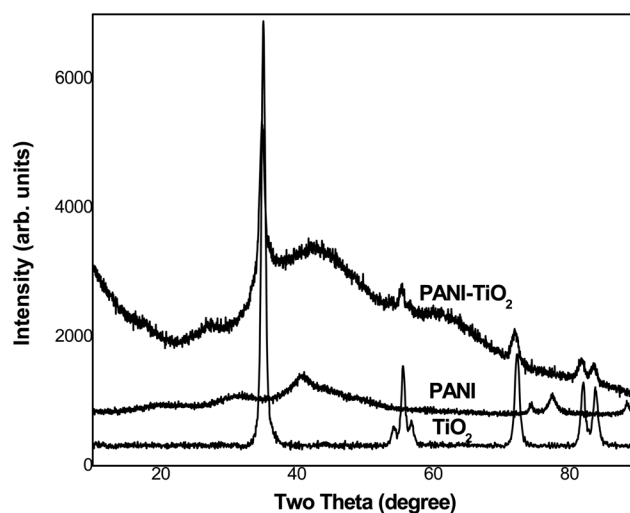Fig. 3 Optical UV-Vis data for (a) PANI and (b) PANI-TiO$_2$ NPs.

Fig. 4 XRD data from PANI, TiO$_2$ and PANI-TiO$_2$ NPs.

NPs indicates the predominance of TiO_2 in the composite; the anatase phase (101) of TiO_2 has remained, while the broad weak peaks of PANI have slightly shifted. All these suggest that there might be interaction between PANI and TiO_2 due to the microwave irradiation effect during NP development. Applying the Scherrer formula, eqn (A), to the most prominent sharp peak at 35°, the size of the crystallite t was obtained as 20 nm:

$$t = k\lambda/b \cos\theta, \tag{A}$$

where, b is the breadth in radians, θ is the Bragg angle and λ is the wavelength of radiation. The coefficient k normally takes a value close to 0.9.

Application: detection of 1,2-DAB using PANI-TiO$_2$ NPs

The potential application of PANI-TiO_2 NPs on GCE using Nafion is to develop a selective and sensitive electrochemical sensor. The synthesized PANI-TiO_2 NPs were deposited onto GCE as a layer of thin film to yield the working electrode of the desired electrochemical sensor. The stability of the thin film of NPs on GCE was enhanced by the addition of a drop of Nafion, a copolymer with its own electrical conductivity. As a result, the use of Nafion improved the conductance of the fabricated working electrode based on PANI-TiO_2 NPs/binder/GCE, as well as the electron transfer rate from sensing medium to sensor. Similar results have been reported by earlier authors in the detection of toxic chemicals using the electrochemical ($I–V$) approach.[28–33] As per the authors' knowledge, the GCE with the synthesized PANI-TiO_2 NPs is the first 1,2-DAB sensor to apply the $I–V$ approach in phosphate buffer phase. The holding time in the Keithley electrometer was set as 1.0 s throughout the experiment.

At the initial phase of this study, the environmental toxic chemicals, namely, 1,2-DAB, 2,4-DAP, 2,4-DAPDHCl, 2,4-DNP, 2-AP, 3,4-DAT, 3-MP, 4-AP, PHyd and p-NP, were subjected to $I–V$ analysis at 0.01 μM and potential of 0 V to +1.5 V in PBS medium (pH 7.0). As presented in Fig. 5(a), 1,2-DAB exhibited the highest current response among the all toxic chemicals, and based on this highest $I–V$ outcome, 1,2-DAB was considered as the
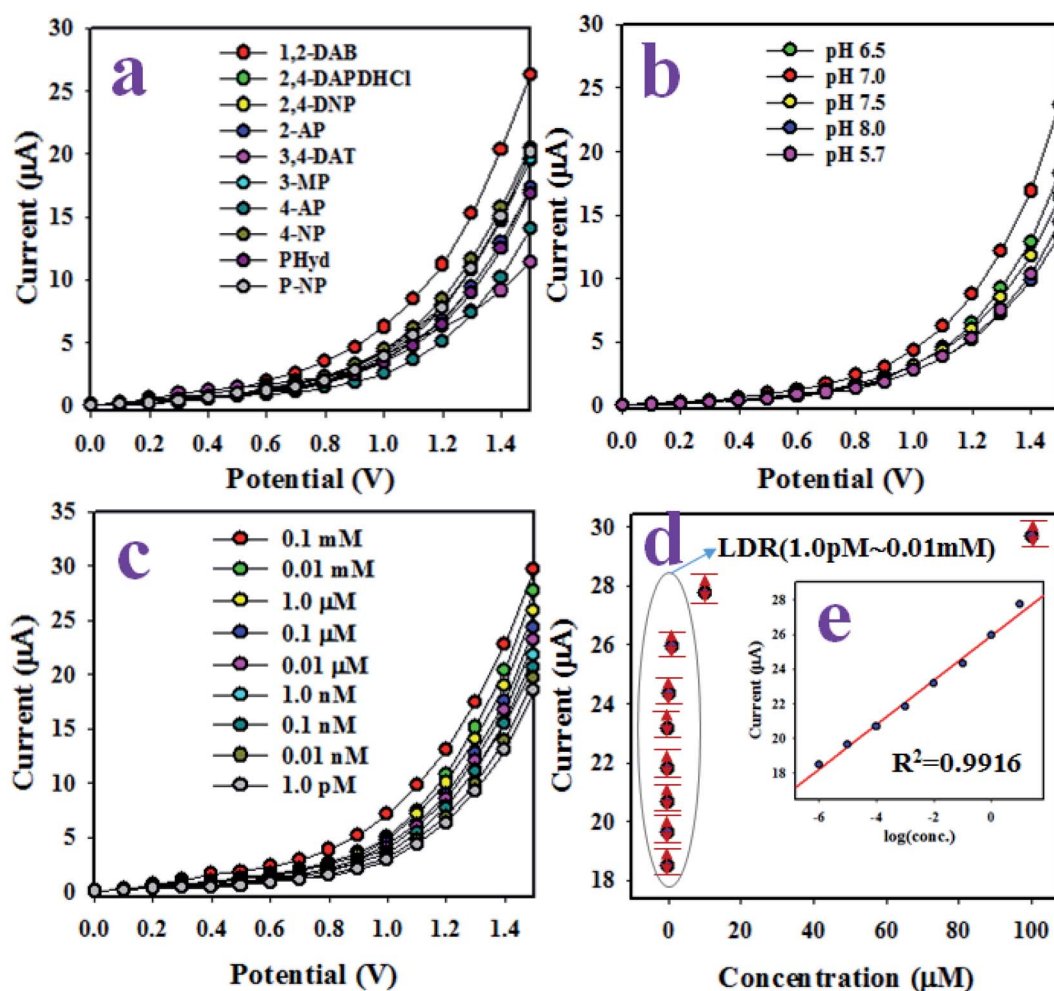

Fig. 5 Electrochemical characterization of the 1,2-DAB sensor based on PANI-TiO$_2$ NPs/Nafion/GCE. (a) The selectivity of the sensor with 0.01 μM concentrations of analyte in the buffer phase, (b) the optimization of pH of the buffer phase for the sensor assembly at 0.01 μM 1,2-DAB, (c) the electrochemical ($I–V$) responses of the sensor based on concentrations of 1,2-DAB ranging from 0.1 mM to 1.0 pM, and (d) the calibration of the 1,2-DAB sensor [inset, current vs. log(conc.)].

selective toxin for the sensor assembly. The synthesized PANI-TiO_2 NPs on GCE do not show equal electrochemical activities in the buffer solutions with different pH values. Thus, pH optimization for the 1,2-DAB sensor based on PANI-TiO_2NPs/Nafion/GCE was executed by the electrochemical analysis of 1,2-DAB at 0.01 μM in a range of buffer pH values, as illustrated in Fig. 5(b). It is clearly shown in Fig. 5(b) that the proposed 1,2-DAB sensor exhibits the highest I–V response in pH 7.0 buffer. Then, the detailed electrochemical analysis of 1,2-DAB sensor was performed to detect 1,2-DAB with a range of concentration of 0.1 mM to 1.0 pM, as demonstrated in Fig. 5(c). This experiment was tested in pH 7.0 buffer. As shown in Fig. 5(c), the resulting I–V responses are distinct and can be separated from each other from low to high concentration of 1,2-DAB. In other words, the I–V outcomes of the 1,2-DAB sensor varied with the concentration of analyte (1,2-DAB) in the detection process. Similar results have been reported in previous articles to detect numerous toxic chemicals and biochemicals applying the I–V approach.[34–41] To establish the calibration of 1,2-DAB sensor, the current data shown in Fig. 5(b) were isolated at the potential

of +1.5 V, and a new calibration curve is plotted from the linear relation of the current *versus* concentration of 1,2-DAB, as shown in Fig. 5(c). As apparent in Fig. 5(c), the current data are linearly distributed from 1.0 pM to 0.01 mM of 1,2-DAB, and this range of concentration is defined as the linear dynamic range (LDR) of the 1,2-DAB sensor to detect 1,2-DAB in pH 7.0 buffer. Obviously, the obtained LDR is a wider concentration range.

For evidence of the linearity of LDR, current *versus* log(-conc.), illustrated in Fig. 5(d) (inset), is plotted, which is satisfied by the regression coefficient $R^2 = 0.9916$, proving the linearity of LDR. The sensitivity of the 1,2-DAB sensor with PANI-TiO_2 NPs/Nafion/GCE, which is calculated from the slope of the calibration curve, is equal to 19.8165 μA μM^{-1} cm^{-2}, a value that is appreciable. Applying a signal-to-noise ratio of 3, the lower limit of detection (DL) of 1,2-DAB sensor was estimated and is equal to 0.93 ± 0.05 pM, an appreciable lower limit of detection.

The reproducibility investigation of an electrochemical sensor offers information about its capability to analyze real
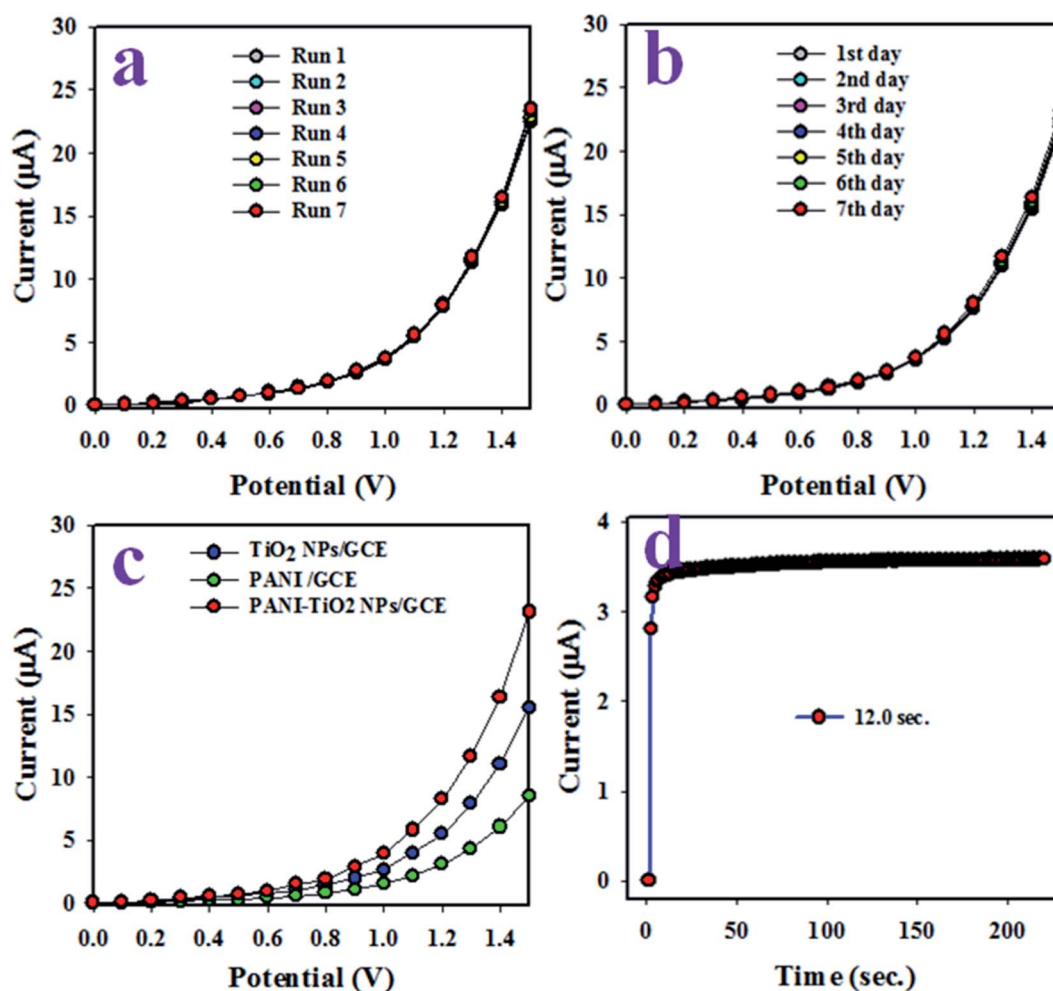

Fig. 6 Optimization of the sensor electrochemical parameters. (a) Reproducibility tests executed under identical conditions of concentration, buffer pH, and applied potential. (b) The validity of the 1,2-DAB sensor over 7 days under similar conditions. (c) A comparison of studies of sensors modified with PANI, TiO_2 NPs and PANI-TiO_2 NPs, and (d) the sensor response time.
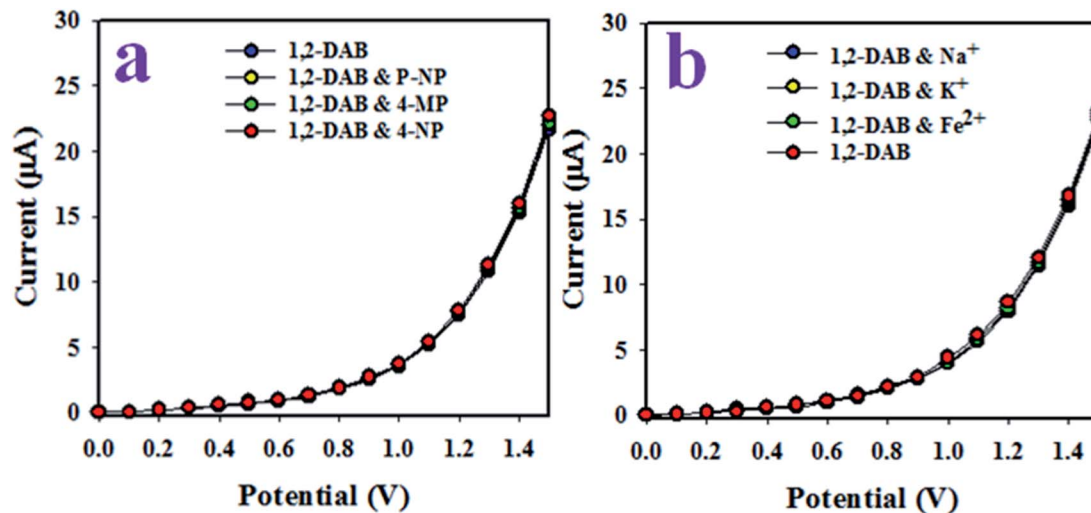
Fig. 7 Interference effects on the 1,2-DAB sensor in the presence of (a) organic and (b) inorganic toxic substances.

samples with constancy in outcome. To determine this parameter, electrochemical analysis was carried out with identical solutions of 0.01 μM 1,2-DAB and under the potential of 0 V to +1.5 V in pH 7.0 buffer, as demonstrated in Fig. 6(a). From the observation of Fig. 6(a), the seven analyses are almost identical, and the intensity of current response is not significantly changed even with washing of the fabricated electrode after each run. The accuracy of current data of the reproducibility test at +1.5 V was investigated and was exhibited to be 1.25% RSD (RSD: relative standard deviation). Thus, this test confirms the reliability of the 1,2-DAB sensor to analyze real environmental samples efficiently. A similar reproducibility test over seven days was made with 0.1 μM concentration of 1,2-DAB at the potential of 0 V to +1.5 V and is presented in Fig. 6(b). As apparent from Fig. 6(b), the electrochemical responses are not distinguishable, as in Fig. 6(a). The results indicate that the synthesized electrode can accomplish identical outcomes over a long-term period with high efficiency. The synthesized NPs consist of two parts, organic PANI and TiO_2 metal oxide. Thus,

GCE was modified with PANI and TiO_2 NPs and subjected to I–V analysis with 0.01 μM 1,2-DAB, which was then compared with PANI-TiO_2 NPs, as illustrated in Fig. 6(c). As shown in Fig. 6(c), the electrode made with PANI-TiO_2 NPs shows superior I–V outcome compared to the others. This is because of the combinational electrochemical effects of PANI and TiO_2 NPs. The response time of a sensor is defined as the time required to complete an I–V analysis. Fig. 6(d) represents the response time of the proposed 1,2-DAB electrochemical sensor, and a very efficient response time (12.0 s) is obtained.

The test of interference effects on an electrochemical sensor is an important measurable feature. This test, based on the PANI-TiO_2 NPs/binder/GCE electrochemical probe, was conducted at 0.01 μM concentration of 1,2-DAB, 4-nitrophenol, p-nitrophenol, and 4-methoxyphenol, as presented in Fig. 7(a). As seen from Fig. 7(a), the current responses were indistinguishable, providing evidence that the electrochemical responses of 1,2-DAB are not affected by the presence of other toxic chemicals. Similar tests were conducted in the I–V analysis of 1,2-DAB
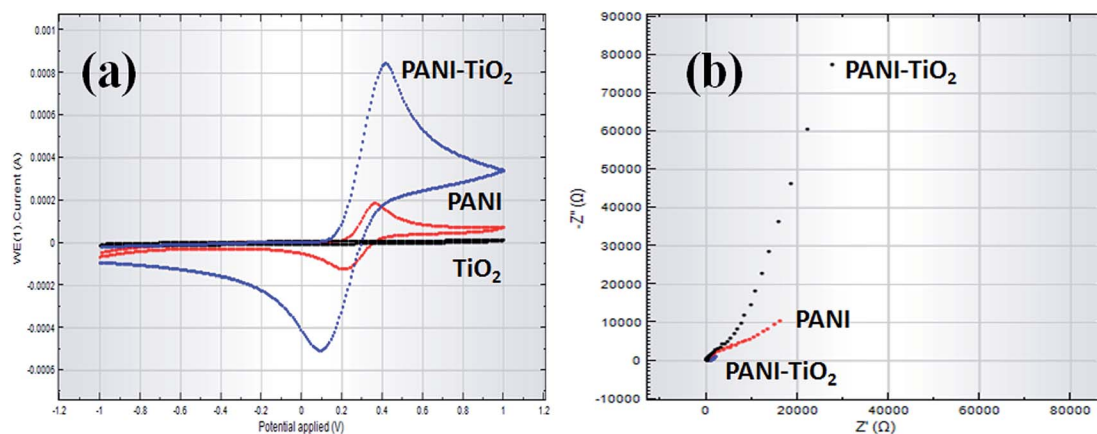

Fig. 8 (a) Cyclic voltammograms and (b) Nyquist (EIS) plots comparing PANI-TiO_2 NPs/binder/GCE, PANI/binder/GCE, and TiO_2/binder/GCE at pH = 7.0 in 0.1 M PBS.

Table 1 The performance of the 1,2-DAB sensor compared to different modifications of working electrodes using the electrochemical method[a]

| Modified electrode	Analyte	DL	LDR	Sensitivity	Ref.
Fe$_3$O$_4$@f-MWCNTs	1,2-DAB	50.00 μM	0.6–80 μM	2.80 μA μM^{-1} cm^{-2}	24
MCM-41/Nafion/GCE	1,2-DCB	13.0 pM	0.089 nM to 8.9 mM	0.7468 μA μM^{-1} cm^{-2}	41
ZnO/CB NCs/GCE	Benzaldehyde	18.75 pM	0.1 nM to 0.1 mM	5.0633 μA μM^{-1} cm^{-2}	42
FeO/CdO NCs/GCE	1,2-DCB	72.73 pM	0.089 nM to 0.89 mM	1.3054 μA μM^{-1} cm^{-2}	43
PANI-TiO$_2$ NPs/GCE	1,2-DAB	0.93 pM	0.1 pM to 0.01 mM	19.817 μA μM^{-1} cm^{-2}	This work

[a] DL (detection limit), LDR (linear dynamic range), nM (nanomole), μM (micromole), pM (picomole).

in the presence of Na$^+$, K$^+$ and Fe^{2+}, illustrated in Fig. 7(b), which shows analogous results to Fig. 7(a). Therefore, the 1,2-DAB sensor based on PANI-TiO$_2$ NPs/binder/GCE is highly selective to 1,2-DAB, and it does not show any interference effects under the presence of other toxic substances (both organic and inorganic).

Before recommending PANI-TiO$_2$ NPs/binder/GCE as an efficient sensor probe material for the selective detection of analytes, it was essential to unveil the electrochemical behaviors as well as impedance properties of PANI-TiO$_2$ in the PANI-TiO$_2$ NPs/binder/GCE assembly by comparing the performance with only PANI, as well as TiO$_2$, in K$_3$[Fe(CN)$_6$] with 0.1 M PBS. For this purpose, initially, bare GCE was fabricated separately with PANI, TiO$_2$, and PANI-TiO$_2$ composite materials by using the conductive coating Nafion binder. The electrochemical behavior of the PANI-TiO$_2$ NPs/binder/GCE sensor probe was studied in K$_3$[Fe(CN)$_6$] and 0.1 M PBS by cyclic voltammetry, which is presented in Fig. 8(a). Here, the PANI-TiO$_2$ NPs/binder/GCE fabricated electrode exhibited the highest current compared to the PANI- as well as TiO$_2$-coated GCE electrodes. Thus, the PANI-TiO$_2$ NPs/binder/GCE fabricated sensor probe exhibited the highest electrochemical activity. Next, the EIS spectra (5.0 mM K$_3$[Fe(CN)$_6$] in 0.1 M PBS, pH = 7.0) were

recorded to explore the relative EIS properties of the PANI-TiO$_2$-coated GCE electrode by adjusting an excitation potential of +0.38 V between 0.1 Hz and 0.1 MHz frequency, as shown in Fig. 8(b). The complex plane plots displayed in Fig. 8(b) indicate that the PANI-TiO$_2$ NPs/binder/GCE exhibits less capacitive current as well as lower impedance compared to only PANI- and TiO$_2$-coated GCE electrodes in 0.1 M PBS/K$_3$[Fe(CN)$_6$]. The less capacitive nature with lower impedance of the PANI-TiO$_2$ NPs/binder/GCE sensor suggests that the electron-transfer ability of the PANI-TiO$_2$ NPs/binder/GCE electrode was significantly improved in the presence of PANI-TiO$_2$ coating, while PANI-TiO$_2$ was bonded onto the surface of GCE. Thus, such electronic property of the modified CGE suggests that PANI-TiO$_2$ NPs/binder/GCE sensor probe perhaps can enhance the electrochemical process. Finally, it is concluded that good electrochemical performance was exhibited by the PANI-TiO$_2$ NPs/binder/GCE modified electrodes compared to only PANI and TiO$_2$, which confirmed the PANI-TiO$_2$ NPs/binder/GCE as the best electrode to be used for the chemical sensing applications.

A comparison of chemical sensors fabricated based on various nanostructured materials is presented in Table 1, and the 1,2-DAB sensor based on PANI-TiO$_2$ NPs/binder/GCE shows appreciable results.
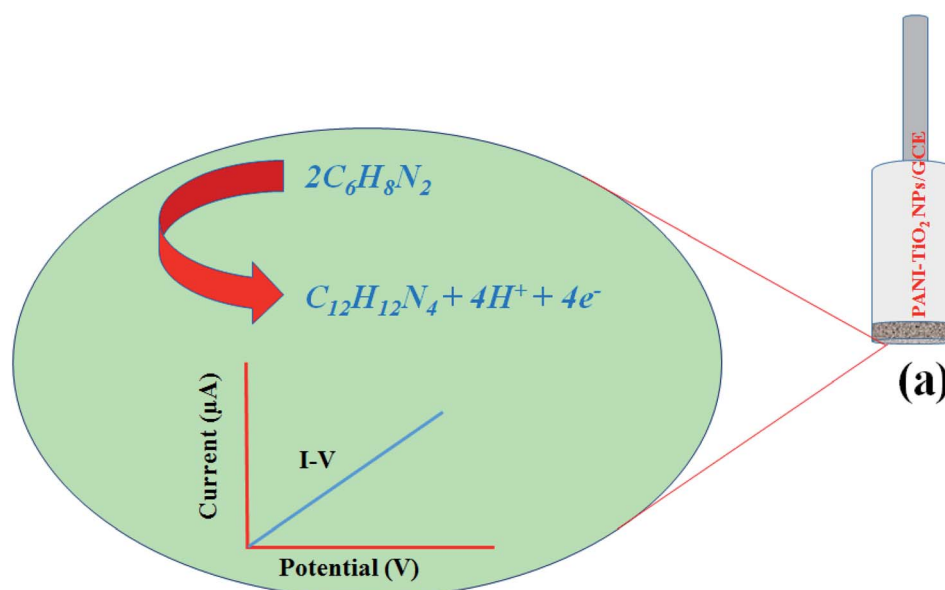

Scheme 1 A graphical view of the oxidation of 1,2-DAB by the fabricated PANI-TiO$_2$ NPs/binder/GCE sensor probe.

Table 2 The analysis of real environmental samples using the PANI-TiO$_2$ NPs/binder/GCE chemical sensor *via* a recovery method[a]

Sample	Added 1,2-DAB concentration (μM)	Measured 1,2-DAB conc.[n] by PANI-TiO$_2$ NPs/binder/GCE (μM)			Average recovery[b] (%)	RSD[c] (%) ($n = 3$)
		R1	R2	R3		
Industrial effluent	0.01000	0.00992	0.00985	0.00964	98.02	1.49
PC-baby bottle	0.01000	0.01005	0.01005	0.01006	100.52	0.06
PC-water bottle	0.01000	0.009859	0.009895	0.00993	98.96	0.36
PVC-food packaging bag	0.01000	0.009982	0.009935	0.009787	99.01	1.03

[a] Mean of three repeat determinations (signal to noise ratio: 3) by the PANI-TiO$_2$ NPs/binder/GCE sensor probe. [b] Concentration of 1,2-DAB determined/concentration taken (unit: μM). [c] Relative standard deviation value indicates precision among three repeat measurements (R1, R2, R3).

The pictorial representation of the sensing mechanism of the PANI-TiO$_2$ NPs/binder/GCE electrode for 1,2-DAB is presented in Scheme 1. In this approach, the oxidation performance of 1,2-DAB is presented according to the reaction (i), as given below.

$$2C_6H_8N_2 \rightarrow C_{12}H_{12}N_4 + 4H^+ + 4e^- \qquad (i)$$
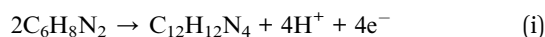
The analogous electrochemical oxidation of 1,2-DAB has been previously reported in various scientific articles.[24,44] As observed from the electrochemical oxidation of 1,2-DAB, electrons are usually generated, which are responsible for higher conductivity in the presence of selective chemicals in the buffer phase. At the beginning of the 1,2-DAB sensing experiment, a few molecules of 1,2-DAB are absorbed on the surface of the GCE modified by PANI-TiO$_2$ NPs, and the corresponding oxidation of 1,2-DAB occurs as stated. With time, the number of absorbed molecules (1,2-DAB) are increased, as well as the oxidation reactions. By the further increasing the number of analyte molecules, the surface of the working electrode approaches its saturation. Again, with the increased number of molecules, a steady-state current concentration in the sensing buffer phase is observed, generating an *I–V* response in the Keithley electrometer. The steady-state *I–V* data are illustrated in Fig. 5(c). Fig. 6(d) shows the response time of 1,2-DAB sensor is 12.0 s, indicating that the 1,2-DAB sensor needs 12.0 s to generate a steady-state *I–V* response. Subsequently, the 1,2-DAB electrochemical sensor based on PANI-TiO$_2$ NPs/binder/GCE showed highly satisfactory outcomes, such as sensitivity (19.8165 μA μM^{-1} cm^{-2}), detection limit (0.93 ± 0.05 pM), and linear dynamic range (1.0 pM to 0.01 mM). Besides this, it was found as highly reproducible and reliable in analyzing real environmental samples with a very short response time.

Analysis of real environmental samples

The 1,2-DAB electrochemical sensor was fabricated with PANI-TiO$_2$ NPs onto GCE using Nafion conducting binder and implemented to detect 1,2-DAB in real environmental samples using the recovery method. The environmental samples were obtained as extracts from PC-baby bottle, PC-water bottle, PVC-food packaging bag, and waste effluent collected from the industrial region of Jeddah, KSA. The corresponding electrochemical analysis data are presented in Table 2. As observed from Table 2, the recoveries of 1,2-DAB are quite satisfactory and acceptable.

Conclusions

Here, PANI-TiO$_2$ NPs were synthesized using a microwave-accelerated reaction system for the development of a selective chemosensor. The synthesized PANI-TiO$_2$ NPs were deposited on a GCE as a thin film using Nafion as the conducting binder, resulting in a working electrode for the desired 1,2-DAB sensor, which was subsequently applied to detect 1,2-DAB in the phosphate buffer phase. After detailed investigations, the 1,2-DAB sensor was found to be highly sensitive over a broad concentration range with a noticeably lower limit of detection; it was reproducible, showing high precision as well as being efficient and having a quick response time, along with the ability to perform over a long period in the buffer phase. Finally, the assembled 1,2-DAB sensor was validated for the detection of 1,2-DAB in real environmental samples and found quite satisfactory. Thus, this is a prospective approach for the development of sensors applying the *I–V* technique.

Conflicts of interest

There are no conflicts to declare.

Acknowledgements

References

1 Y. Shi, L. Peng, Y. Ding, Y. Zhao and G. Yu, Nanostructured conductive polymers for advanced energy storage, *Chem. Soc. Rev.*, 2015, **44**, 6684–6696.

2 Y. Shi, L. Peng and G. Yu, Nanostructured conducting polymer hydrogels for energy storage applications, *Nanoscale*, 2015, 7, 12796–12806.

3 C. Zhan, G. Yu, Y. Lu, L. Wang, E. Wujcik and S. Wei, Conductive polymer nanocomposites: a critical review of

modern advances devices, *J. Mater. Chem. C*, 2017, **5**, 1569–1585.

4 H. D. Tran, J. M. D"Arcy, Y. Wang, P. J. Beltramo, V. A. Strong and R. B. Kaner, The oxidation of aniline to produce "polyaniline": a process yielding many different nanoscale structures, *J. Mater. Chem.*, 2011, **21**, 3534–3550.

5 C. O. Baker, X. Huang, W. Nelson and R. B. Kaner, Polyaniline nanofibers: broadening applications for conducting polymers, *Chem. Soc. Rev.*, 2017, **46**, 1510–1525.

6 L. Wang, X. Lu, S. Lei and Y. Song, Graphene-based polyaniline nanocomposites: preparation, properties and applications, *J. Mater. Chem. A*, 2014, **2**, 4491–4509.

7 T. Sen, S. Mishra and N. G. Shimpi, Synthesis and sensing applications of polyaniline nanocomposites: a review, *RSC Adv.*, 2016, **6**, 42196–42222.

8 V. Gilja, K. Novaković, J. Travas-Sejdic, Z. Hrnjak-Murgić, M. K. Roković and M. Žic, Stability and Synergistic Effect of Polyaniline/TiO$_2$ Photocatalysts in Degradation of Azo Dye in Wastewater, *Nanomaterials*, 2017, **7**, 412.

9 T. Gichner, D. A. Stavreva and F. V. Breusegem, *O*-Phenylenediamine-induced DNA damage and mutagenicity in tobacco seedlings is light-dependent, *Mutat. Res., Genet. Toxicol. Environ. Mutagen.*, 2001, **495**, 117–125.

10 J. H. Li, D. Z. Kuang, Y. L. Feng and M. Q. Liu, Voltammetric etermination of ophenylenediamine in industrial wastewater by an electrode modified with nanocomposite film of TiO$_2$/hydroxyapatite/MWCNT, *Chin. J. Anal. Chem.*, 2011, **39**, 1864–1870.

11 M. Matsumoto, M. Suzuki, H. Kano, S. Aiso, K. Yamazaki and S. Fukushima, Carcinogenicity of *ortho*-phenylenediamine dihydrochloride in rats and mice by two-year drinking water treatment, *Arch. Toxicol.*, 2012, **86**, 791–804.

12 N. Li, Y. Gua, M. Gao, Z. Wang, D. Xiao, Y. Li, R. Lin and H. He, Colorimetric determination of *o*-phenylenediamine in water samples based on the formation of silver nanoparticles as a colorimetric probe, *Spectrochim. Acta, Part A*, 2015, **140**, 328–333.

13 S. C. Rastogi, A method for the analysis of intermediates of oxidative hair dyes in cosmetic products, *J. Sep. Sci.*, 2001, **24**, 173–178.

14 S. P. Wang and T. H. Huang, Separation and determination of aminophenols and phenylenediamines by liquid chromatography and micellar electrokinetic capillary chromatography, *Anal. Chim. Acta*, 2005, **534**, 207–214.

15 S. Bilal and R. Holze, *In situ* UV-vis spectroelectrochemistry of poly (ophenylenediamine-*co-m*-toluidine), *Electrochim. Acta*, 2007, **52**, 5346–5356.

16 S. Dong, L. Chi, S. Zhang, P. He, Q. Wang and Y. Fang, Simultaneous determination of phenylenediamine isomers and dihydroxybenzene isomers in hair dyes by capillary zone electrophoresis coupled with amperometric detection, *Anal. Bioanal. Chem.*, 2008, **391**, 653–659.

17 N. Li, Y. Gu, M. Gao, Z. Wang, D. Xiao, Y. Li, R. Lin and H. He, Colorimetric determination of *o*-phenylenediamine in water samples based on the formation of silver nanoparticles as a colorimetric probe, *Spectrochim. Acta, Part A*, 2015, **140**, 328–333.

18 R. Das, C. D. Vecitis, A. Schulze, B. Cao, A. F. Ismail, Z. Luk, J. Chen and S. Ramakrishna, Recent advances in nanomaterials for water protection and monitoring, *Chem. Soc. Rev.*, 2017, **46**, 6946–7020.

19 M. Saleem and K. H. Lee, Optical sensor: A promising strategy for environmental and biomedical monitoring of ionic species, *RSC Adv.*, 2015, **5**, 72150–72287.

20 Y. N. Zhang, Q. Niu, Z. Gu, N. Yang and G. Zhao, Recent progress on carbon nanomaterials for the electrochemical detection and removal of environmental pollutants, *Nanoscale*, 2019, **11**, 11992–12014.

21 M. Govindhan, B. R. Akhikari and A. Chen, Nanomaterials-based electrochemical detection of chemical contaminants, *RSC Adv.*, 2014, **4**, 63741–63760.

22 S. A. Hira, M. Nallal and K. H. Park, Fabrication of PdAg nanoparticle infused metal-organic framework for electrochemical and solution-chemical reduction and detection of toxic 4-nitrophenol, *Sens. Actuators, B*, 2019, **298**, 126861.

23 S. Wang, A. Ramachandran and S. J. Ja, Integrated microring resonator biosensors for monitoring cell growth and detection of toxic chemicals in water, *Biosens. Bioelectron*, 2009, **24**, 3061–3066.

24 R. Sasikumar, P. Ranganathan, S. M. Chen, S. P. Rwei and Muthukrishnan, Electro-oxidative determination of aromatic amine (*o*-phenylenediamine) using organic–inorganic hybrid composite, *J. Colloid Interface Sci.*, 2017, **504**, 149–157.

25 C. Zhao, Z. Jiang, R. Mu and Y. Li, A novel sensor for dopamine based on the turn-on fluorescence of Fe-MIL-88 metal–organic frameworks–hydrogen peroxide-ophenylenediamine system, *Talanta*, 2016, **159**, 365–370.

26 M. Khalid, M. A. Tumelero, V. C. Zoldan, C. C. P. Cid, D. F. Franceschini, R. A. Timm, L. T. Kubota, S. A. Moshkalev and A. A. Pasa, Polyaniline nanofibers-graphene oxide nanoplatelets composite thin film electrodes for electrochemical capacitors, *RSC Adv.*, 2014, **4**, 34168–34178.

27 D. Chaudhuri and D. D. Sarma, Blue emitting polyaniline, *Chem. Commun.*, 2006, 2681–2683.

28 O. Simoska and K. J. Stevenson, Electrochemical sensors for rapid diagnosis of pathogens in real time, *Analyst*, 2019, **144**, 6461–6478.

29 C. Gao, Z. Guo, J. H. Liu and X. J. Huang, The new age of carbon nanotubes: An updated review of functionalized carbon nanotubes in electrochemical sensors, *Nanoscale*, 2012, **4**, 1948–1963.

30 X. Ke, Micro-fabricated electrochemical chloride ion sensors: From the present to the future, *Talanta*, 2020, **211**, 120734.

31 J. Yin, W. Gao, Z. Zhang, Y. Mai, A. Luan, H. Jin, J. Jian and Q. Jin, Batch microfabrication of highly integrated silicon-based electrochemical sensor and performance evaluation via nitrite water contaminant determination, *Electrochim. Acta*, 2020, **335**, 135660.

32 C. Zhang, J. Ping and Y. Ying, Evaluation of trans-resveratrol level in grape wine using laser-induced porous graphene-

based electrochemical sensor, *Sci. Total Environ.*, 2020, **714**, 136687.

33 D. Tyagi, H. Wang, W. Huang, L. Hu, Y. Tang, Z. Guo, Z. Ouyang and H. Zhang, Recent advances in two-dimensional-materials-based sensing technology toward health and environmental monitoring application, *Nanoscale*, 2020, **12**, 3535–3559.

34 H. Li, P. Gong, J. Jiang, Y. Li, J. Pang, L. Chen and J. Zhao, Organic-inorganic hybrids assembled from plenary Keggin-type germanotungstate units and 3d-4f heterometal clusters, *Dalton Trans.*, 2019, **48**, 3730–3742.

35 C. Anichini, W. Czepa, D. Pakulski, A. Aliprandi, A. Ciesielski and P. Samori, Chemical sensing with 2D materials, *Chem. Soc. Rev.*, 2018, **47**, 4860–4908.

36 Z. Li, Z. Mo, S. Meng, H. Gao, Z. Niu and R. Guo, The construction and application of chiral electrochemical sensors, *Anal. Methods*, 2016, **8**, 8134–8140.

37 A. Rehman and Z. Zeng, Methods and approaches of utilizing ionic liquids as gas sensing materials, *RSC. Adv.*, 2015, **5**, 58371–58392.

38 H. J. Salavagione, A. M. Diez-Pascual, E. Lazaro, S. Vera and M. A. Gomez-Fatou, Chemical sensors based on polymer composites with carbon nanotubes and graphene: the role of the polymer, *J. Mater. Chem. A*, 2014, **2**, 14289–14328.

39 R. K. Kannan, D. J. Late, H. Morgan and C. S. Rout, Recent developments in 2D layered inorganic nanomaterials for sensing, *Nanoscale*, 2015, **7**, 13293–13312.

40 A. Chen and S. Chatterjee, Nanomaterials based electrochemical sensors for biomedical applications, *Chem. Soc. Rev.*, 2013, **42**, 5425–5438.

41 B. M. Abu-Zied, M. M. Alam, A. M. Asiri, W. Schwieger and M. M. Rahman, Fabrication of 1,2-dichlorobenzene sensor based on mesoporous MCM-41 material, *Colloids Surf., A*, 2019, **562**, 161–169.

42 M. M. Rahman, M. M. Alam and A. M. Asiri, Carbon black co-adsorbed ZnO nanocomposites for selective benzaldehyde sensor development by electrochemical approach for environmental safety, *J. Ind. Eng. Chem.*, 2018, **65**, 300–308.

43 M. M. Rahman, M. M. Alam and A. M. Asiri, Sensitive 1,2-dichlorobenzene chemi-sensor development based on solvothermally prepared FeO/CdO nanocubes for environmental safety, *J. Ind. Eng. Chem.*, 2018, **62**, 392–400.

44 C. Zhao, Z. Jiang, R. Mu and Y. Li, A novel sensor for dopamine based on the turn-on fluorescence of Fe-MIL-88 metal–organic frameworks–hydrogen peroxide–ophenylenediamine system, *Talanta*, 2016, **159**, 365–370.